Electronic Supplementary Material (ESI) for Journal of Materials Chemistry A.

Supporting Information

Nanofilament array embedded tungsten oxide for highly efficient electrochromic supercapacitor electrodes

Jongmin Kim,[a] Akbar I. Inamdar ,[a] Yongcheol Jo,[a] Sangeun Cho,[a] Abu Talha Aqueel Ahmed,[a] Bo Hou,[b] SeungNam Cha,[c] Tae Geun Kim,[d] Hyungsang Kim*,[a] & Hyunsik Im*,[a]

[a] *Division of Physics and Semiconductor Science, Dongguk University, Seoul 04620, South Korea*
[b] *Department of Engineering Science, University of Cambridge, Cambridge, CB2 1TN, UK*
[c] *Department of Physics, Sungkyunkwan University, Suwon, 16419, Republic of Korea*
[d] *Department of Electrical Engineering, Korea University, Seoul 02841, South Korea*

** Corresponding authors: hskim@dongguk.edu, hyunsik7@dongguk.edu*

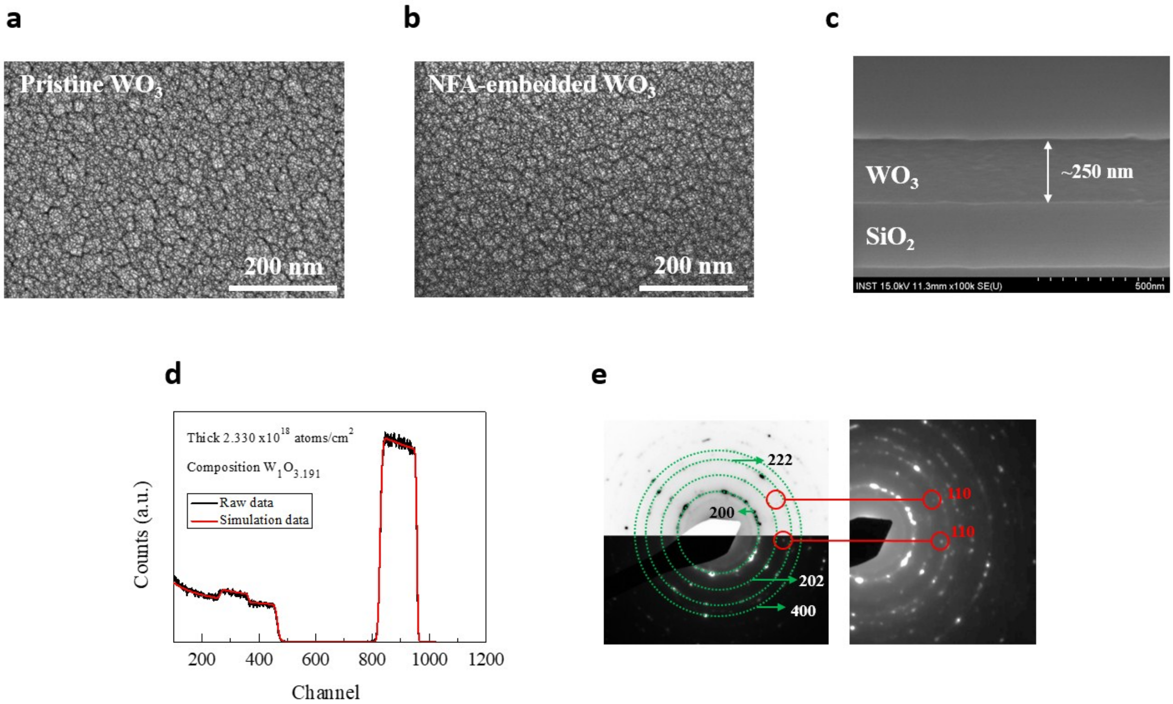

Fig. S1 Top-view field-emission scanning electron microscopy (FE-SEM) images for (a) the pristine WO_3 and (b) NFA-embedded WO_3 films. (c) Cross-sectional FE-SEM image of the WO_3 film. FE-SEM image showing the thickness of the WO_3 film. (d) Rutherford backscattering spectroscopy (RBS) profiles of the WO_3 film. (e) SAED patterns measured after the electroforming process.

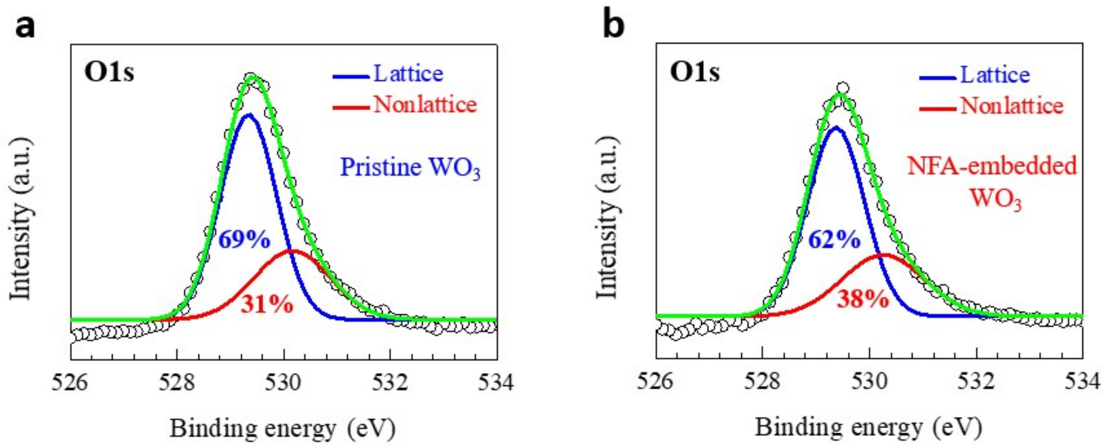

Fig. S2 XPS spectra for O1s peaks in (a) the pristine WO_3 and (b) NFA-embedded WO_3 films.

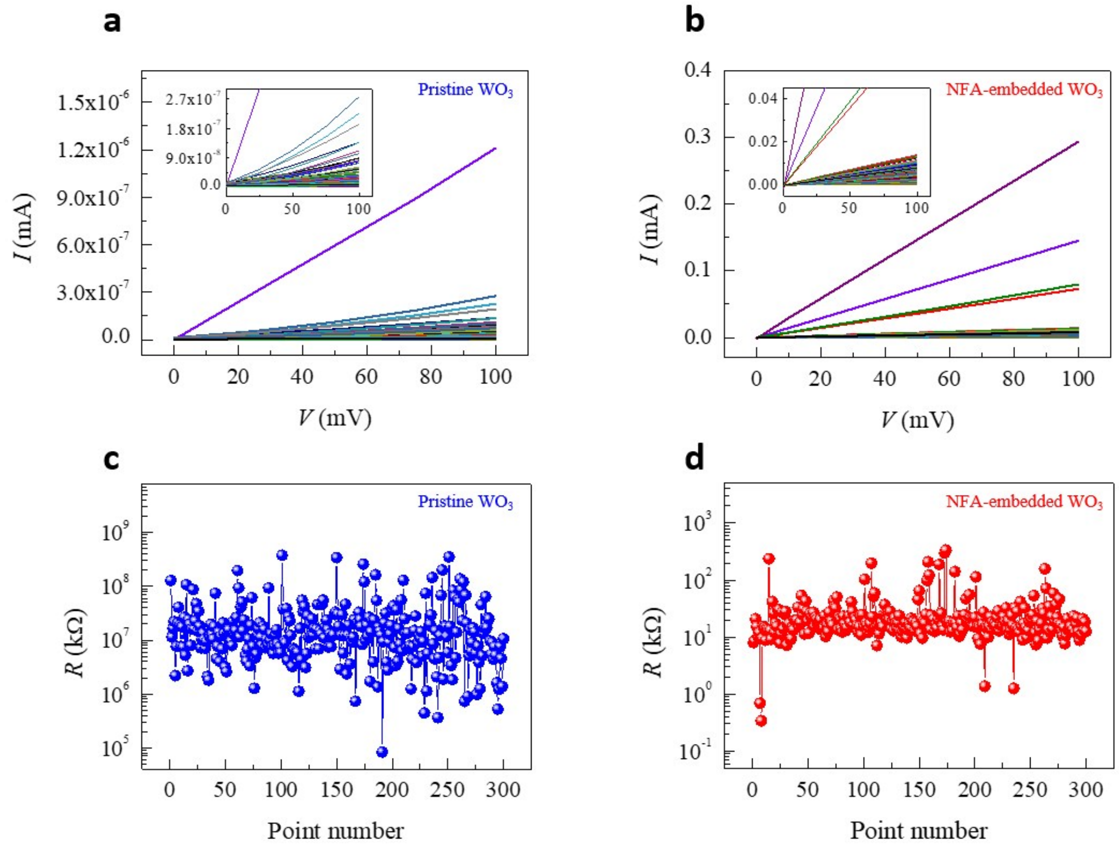

Fig. S3 Two-probe *I-V* characteristics with contacts the WO_3 film and the conducting ITO substrate. (a, b) The measured *I-V* curves for the pristine WO_3 and NFA-embedded WO_3 electrodes. The insets show magnified views of the *I-V* curves. (c, d) The resistance as a function of the point number at 0.1 V read voltage. The resistance ratio between the pristine WO_3 and NFA-embedded WO_3 electrodes more than 6 orders of magnitude.

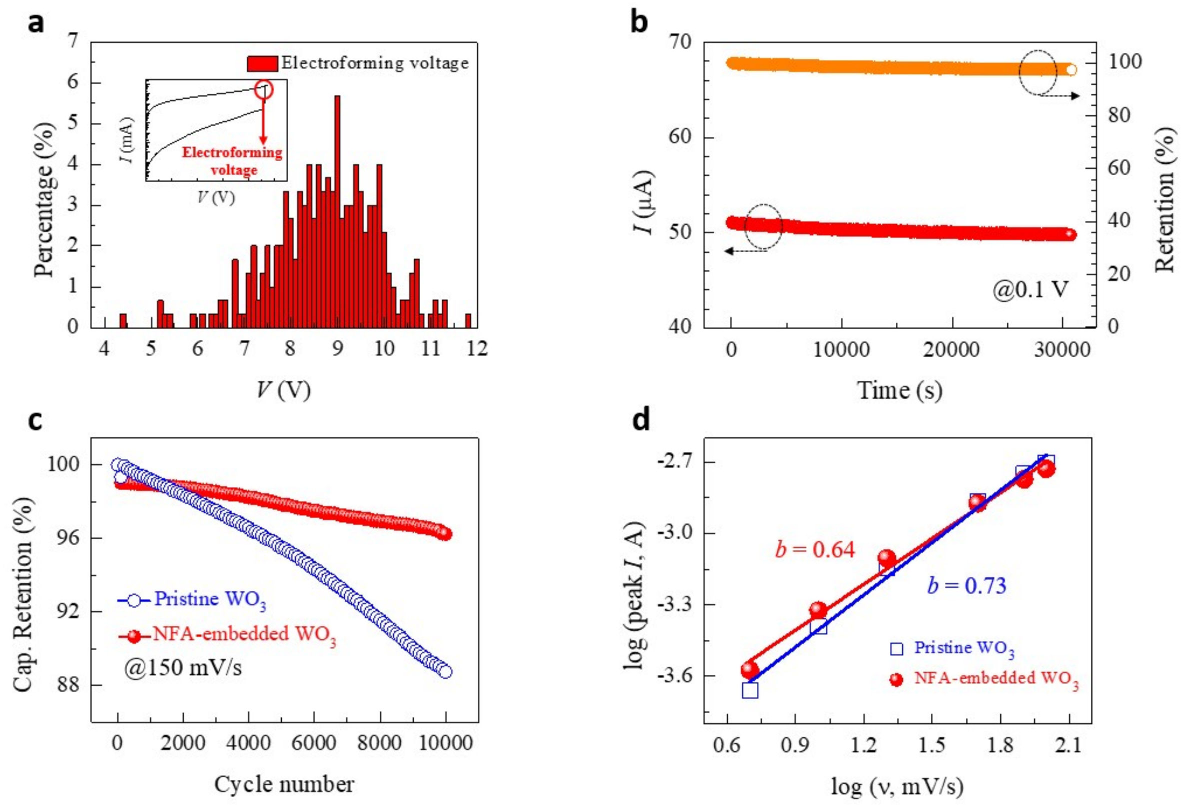

Fig. S4 (a) Distribution of electroforming voltage for the NFA-embedded WO_3 electrode. The inset shows the electroforming voltage. (b) Retention characteristic of the NFA-embedded WO_3 electrode at room temperature and 0.1 V read voltage with almost stable current value. (c) Cycling performance for 10000 cycles at a scan rate of 150 mV s^{-1}. (d) Determination of the *b*-value at scan rates from 5 to 100 mV s^{-1}.

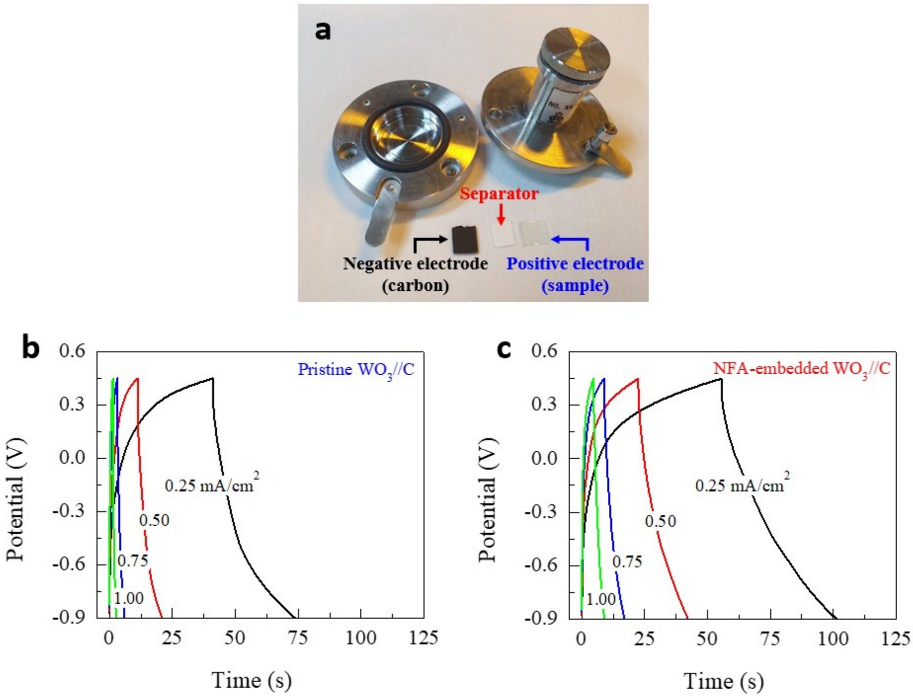

Fig. S5 (a) Photograph showing the asymmetric supercapacitor. The galvanostatic charge–discharge profiles of (b) the pristine WO_3//C and (c) NFA-embedded WO_3//C asymmetric supercapacitor devices at various current densities.

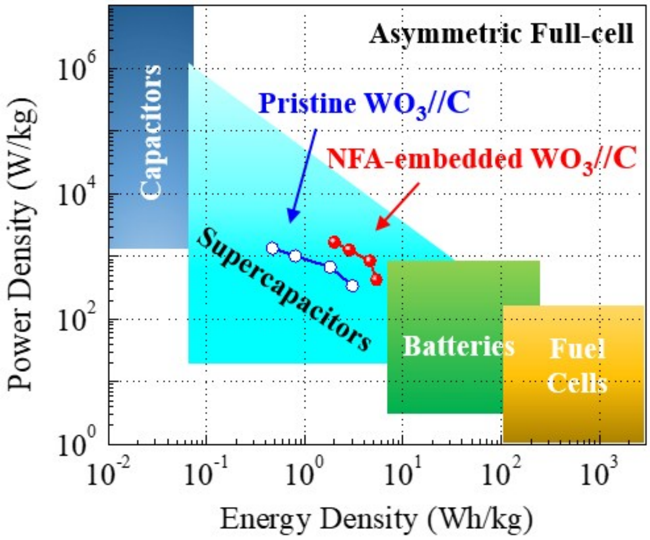

Fig. S6 Energy density vs. power density for the pristine WO_3//C and NFA-embedded WO_3//C asymmetric supercapacitors.

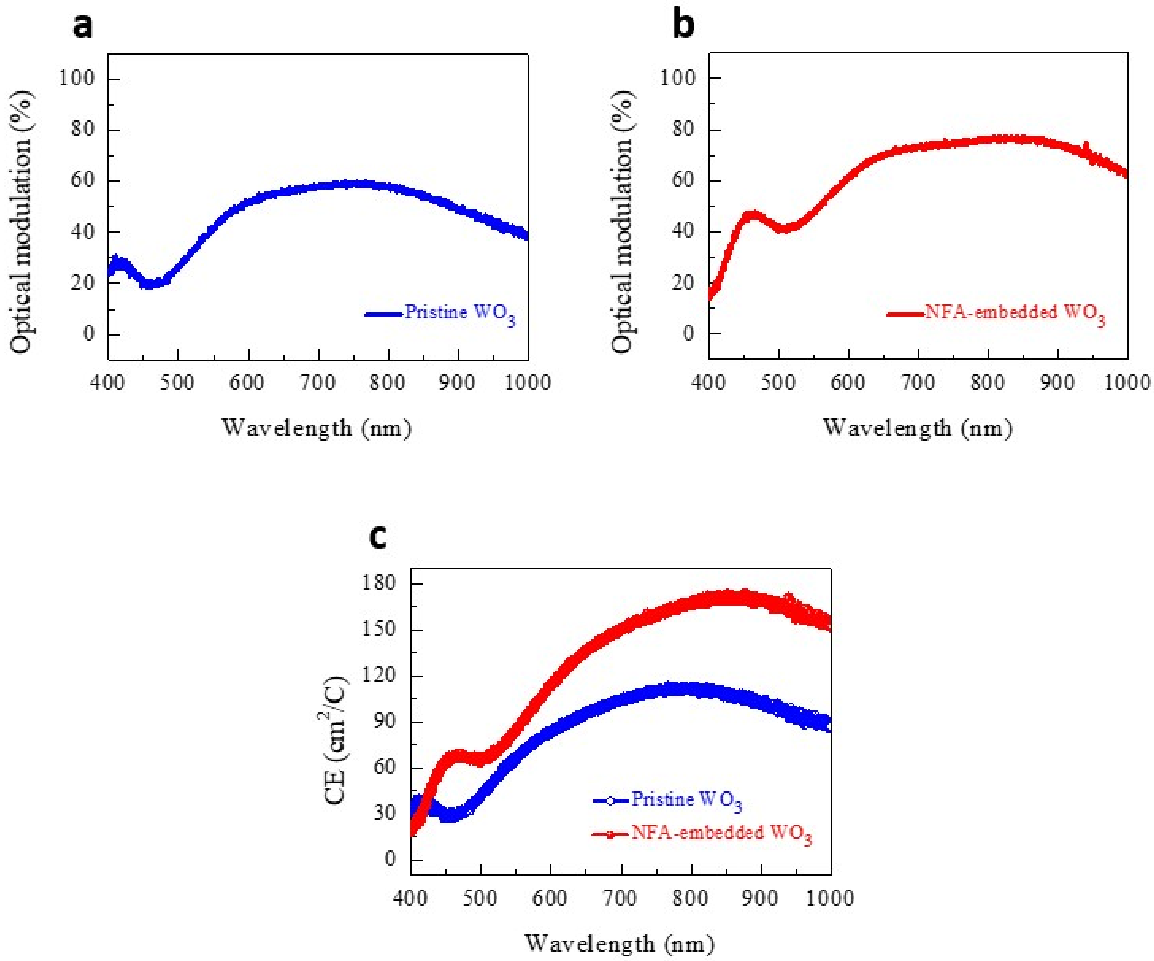

Fig. S7 (a, b) Optical modulation and (c) coloration efficiency for the pristine WO_3 and NFA-embedded WO_3 electrodes.

Table S1 Percentages of different chemical states of W for pristine WO_3 and NFA-embedded WO_3 films.

	Percentages of chemical states of W (%)	
Chemical states	Pristine WO_3	NFA-embedded WO_3
W^0 (Metallic W)	0	12.3
W^{4+} (WO_2)	0	33.6
W^{5+} (W_2O_5)	32.2	10.9
W^{6+} (WO_3)	67.8	43.2